PHYSICAL REVIEW C VOLUME 26, NUMBER 5 NOVEMBER 1982

Low energy antiproton-nucleus interactions

M. R. Clover, R. M. DeVries, N. J. DiGiacomo, and Y. Yariv*
Physics Division, Los Alamos National Laboratory, Los Alamos, New Mexico 87545
(Received 24 May 1982)

The interaction of 175-MeV antiprotons with nuclei is examined within the intranuclear cascade model. The experimental characteristics of nucleon-antinucleon annihilation and scattering are used as input, and the propagation of the resultant pions through the nucleus is treated realistically. The effect of the antiproton-nucleus strong attraction is also included. Overall characteristics of antiproton annihilation within nuclei, particularly the large, well-defined energy deposition, indicate that such collisions constitute a unique laboratory for the study of nuclei at very high excitations. The calculations also identify promising experimental observables and triggers.

[NUCLEAR REACTIONS 175 MeV antiproton-nucleus scattering and annihilations. Intranuclear cascade calculations. Nuclei at high excitations.]

I. INTRODUCTION AND MOTIVATION

There is intense interest in what happens to nuclei and nuclear matter at high densities and temperatures.[1,2] Unfortunately, the ideal laboratory for such studies has yet to be found. Indeed, the very concept of temperature for nuclei (the thermalization of a highly excited collection of nucleons) has little experimental basis to date.[3] Collisions of relativistic and ultrarelativistic heavy ions (RHI) can possibly provide high local matter densities, but because of fragmentation due to conservation of longitudinal momentum, the amount of matter available to thermalize the energy may be small.

Very high energy densities in heavy nuclei might, however, cause the nucleus, or regions of the nucleus, to undergo a transition from a collection of nucleons to a quark-gluon plasma. The structure of the quantum chromodynamics (QCD) vacuum is believed[2] to be such that at energy densities a few times that of the nucleon such a transition might occur. In addition, the simple first-order phase transition from a nuclear fluid to a hot nuclear gas (when the excitation energy E^* of the nucleus becomes greater than the disassembly energy) is quite interesting. There exist, in fact, experimental data that find a plausible interpretation in the latter scenario.[4]

In this work we quantitatively verify suggestions[5,6] that low-energy ($E_{\bar{p}} < 1$ GeV) antinucleon-nucleus annihilations are possibly the best place to study nuclei at high excitation. When an antinucleon annihilates on a nucleon within a nucleus, a large number of pions (at low $\bar{N}$ energies, approximately five) are produced in a hadron-sized region and carry away approximately 2 GeV of energy. The average pion momentum is such that pions are strongly absorbed by nucleons to form Δ_{33} resonances. We choose low energies to keep the longitudinal momentum (and possible fragmentation) to a minimum and to assure that the annihilation region moves rather slowly through the nucleus ($E_{\bar{p}} = 175$ MeV implies that the "fireball" velocity, $\beta_{\bar{N}N}$, is 0.29). Also, at low energy the annihilation is predominately into pions, and at 175 MeV there is no competition from inelastic pion production. The LEAR (Low Energy Antiproton Ring) facility at CERN makes this discussion timely. Indeed, we choose antiprotons and $E_{\bar{p}} = 175$ MeV (600 MeV/c) because approved LEAR experiments[7] will provide data for these conditions. One disadvantage of lower energies is the larger $\bar{N}N$ cross section and subsequent surface localization of annihilations in nuclei. Our calculations confirm earlier observations[8] that the strong antinucleon-nucleus attraction remedies this problem in part and increases significantly the antinucleon penetration of the nucleus.

In what follows, we begin with a discussion of $\bar{p}p$, $\bar{p}n$, and antiproton-nucleus ($\bar{p}$-A) phenomenology. The intranuclear cascade (INC) approach is outlined, and the modifications necessary to consider $\bar{p}$-A collisions are detailed. A broad range of results is then presented and comparisons are made with the few existing data. Since the calculations will be used as "background" in considering high statistics data to come from LEAR, a discussion of the limi-

tations of the INC approach and the physics not contained within the model is aimed at evaluating the significance of disagreements between data and calculation. Finally, promising triggers and potentially revealing observables are identified.

It is apparent that antinucleon-nucleus scattering will be of interest for other reasons, ranging from the search for baryonium states to more conventional nuclear reaction and structure physics.[9] Our calculations should also be of great utility in these investigations.

II. $\bar{p}p$, $\bar{p}n$ PHENOMENOLOGY

In Fig. 1(a), we see the energy dependence of the elements of the $\bar{p}p$ cross section: σ_{tot}, σ_{ann} (annihilation), σ_{el} (elastic), and σ_{cx} (charge exchange, $\bar{p}p \rightarrow \bar{n}n$). The most dramatic features as compared to pp [Fig. 1(b)] are the magnitude of σ_{tot} and the large annihilation component that exists down to zero energy. Few $\bar{p}n$ and $\bar{n}n$ data exist, and to the 10% level it appears that $\sigma_{\bar{p}p} = \sigma_{\bar{p}n} = \sigma_{\bar{n}n} = \sigma_{\bar{n}p}$ for σ_{tot}, σ_{el}, and σ_{ann}. The angular distributions for $\bar{p}p$ are shown in Fig. 2, along with those for pp for a few momenta. Note the striking difference in fall-off with angle. As has been shown,[8] this has important ramifications for Pauli-blocking effects and inelastic scattering.

In considering the data, we find little difference between characteristics of the annihilation from rest up to 500 MeV. We will generally use "at-rest" data, as they are more plentiful. Over 97% of the annihilations are into pions, with less than 3% into kaons. The total pion multiplicity distribution and the momentum distribution of ejectiles in $\bar{p}p$ annihilation are displayed in Fig. 3. Note that the pion momentum distribution peaks at the point where the cross section for formation of the Δ_{33} resonance is a maximum ($\simeq$200 mb).

Information concerning the space-time structure of the annihilation can be gained by examining the correlation between pions produced in the annihilation. Such "pion-interferometry" experiments[10] reveal that the annihilation occurs in a volume of radius $\simeq$1.8 fm with a characteristic coherence length $c\tau \simeq 1.5$ fm. Thus the annihilation is a fast, well-localized process. Statistical phase-space models[11] are relatively successful in describing the characteristics of the annihilation products. We, in fact, use such a model to parametrize the annihilation characteristics for input to the INC code.

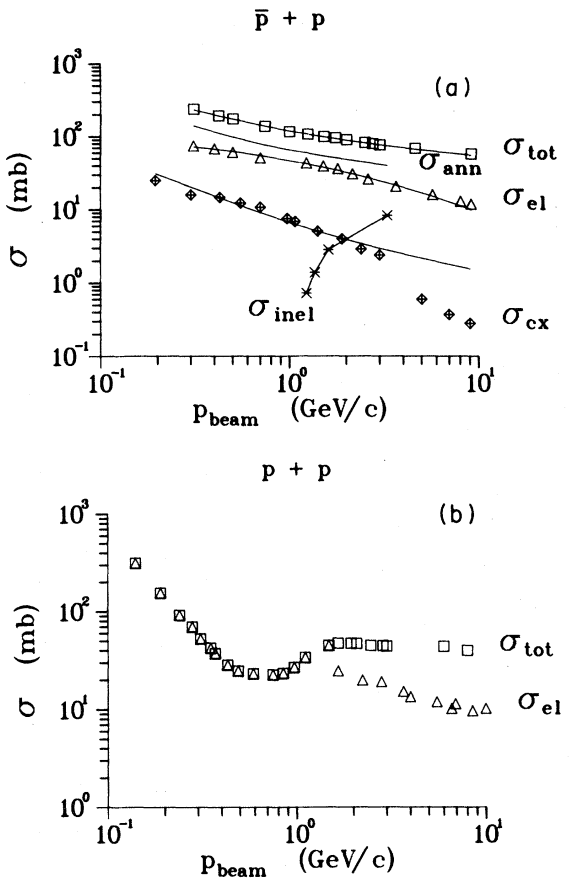

FIG. 1. (a) Composition of the $\bar{p}$-p total cross section vs beam momentum. (b) The p-p total and elastic cross sections vs beam momentum. The solid curves result from the parametrizations used in the calculations [Eqs. (1)–(3)] from the data of Refs. 28 and 29.

III. $\bar{p}$-A PHENOMENOLOGY

Few data exist for $\bar{p}$-A interactions. Early bubble chamber work[12] involving a few hundred events revealed some "stars" with observed charged particle multiplicities up to 16. These violent annihilations, though somewhat rare, indicate that a large amount of the annihilation energy can be transferred to a nucleus. More recently, 484 $\bar{n}$-light nucleus interactions were studied with a bubble chamber at CERN.[13] These data provide a better but still very inadequate picture of the effect of antinucleon annihilation in nuclei. The limited statistics inherent in bubble-chamber or streamer-chamber studies allow only a gross view of the features of the interaction. High-statistics counter experiments are necessary before any quantitative conclusions can be drawn. On the other hand, the bubble/streamer-

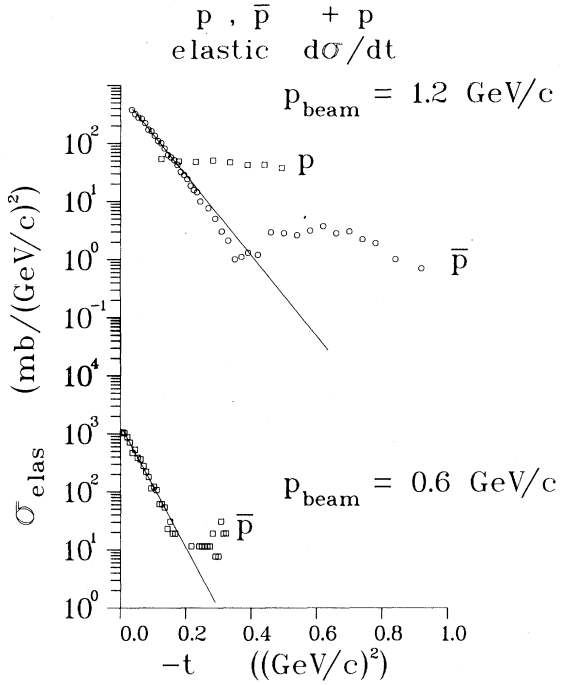

FIG. 2. The $\bar{p}$-p elastic angular distributions at $p_{\text{beam}}=0.6$ and 1.2 GeV/c vs four momentum transfer squared. For comparison, the p-p elastic angular distribution is shown at 1.2 GeV/c. The solid curves result from the parametrizations used in the calculation [Eqs. 4(a) and (b)] from Ref. 29.

chamber measurements do provide a profile of the entire (charged particle) event. In this sense the two approaches are complementary.

There are no useful elastic scattering data for $\bar{p}$-A scattering. Early bubble-chamber work[14] did provide a crude estimation for $\bar{p}$-^{12}C averaged over a broad incident energy range, but poor beam quality has prevented careful measurement. Thus, there is little knowledge of the $\bar{p}$-A optical potential. What is known comes from the study of antiprotonic atoms[15] and the examination of $\bar{p}$-A reaction cross sections.[16] The strong annihilation channel makes the scattering quite diffractive. The very strength of the absorption makes the problem of treating the scattering with standard optical model techniques quite difficult. In addition, there appears to be a very strong attraction between antinucleons and nuclei. It is known that for $\bar{p}p$ and $\bar{p}n$ scattering, the strong attraction stems from the G-parity reversed two pion exchange part of the force.[17] For $\bar{p}$-A scattering, however, the attraction is not easily determined, given the lack of elastic scattering data. Calculations[18] predict a variety of strengths and ranges for the real part of the optical potential. The question awaits LEAR elastic-scattering data for resolution. For our work we take guidance from antiprotonic atom data and recent $\bar{p}$-A absorption cross section data analyzed within the model of Ref. 8, and assume a real potential of depth 250 MeV and a range that follows the matter density. This strong attraction is very important in allowing the $\bar{p}$ to penetrate further into the nucleus. We will discuss this effect quantitatively in Sec. VII B.

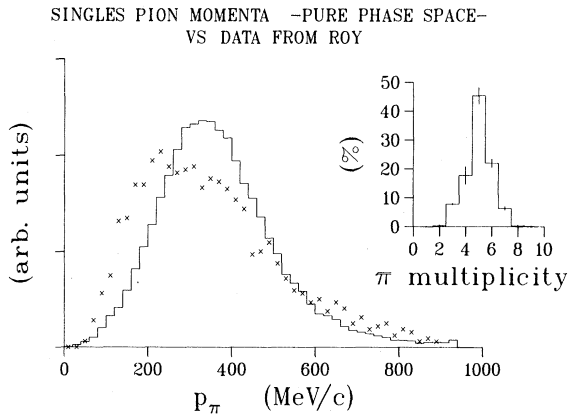

FIG. 3. The momentum distribution of pions emitted in $\bar{p}$-p annihilation at rest ($\times$) along with the results of the phase space model (histogram) used in the calculations (see text). The inset shows the $\bar{p}$-p at rest annihilation pion multiplicity distribution (Ref. 31) used as input for the $\bar{p}$-A calculations.

IV. THE INTRANUCLEAR CASCADE MODEL

The INC approach is quite well documented,[19] and we present here only those considerations relevant to $\bar{p}$-A interactions. We have modified the nucleon-nucleus/nucleus-nucleus INC code ISABEL of Yariv and Fraenkel.[20,21] ISABEL is the state-of-the-art version of a model that has proved quite successful in describing most aspects of hadron-nucleus collisions over a broad incident energy, target mass, and projectile mass range. It is a timelike Monte Carlo program that allows for interactions between cascading particles.[21] It treats pion-nucleon (π-N) interactions in the isobar model and includes an energy dependent width for the delta.[22] The nuclear momentum distribution is assumed to be a Fermi gas within the local density approximation (LDA). Depletion of the Fermi sea as the interaction proceeds is taken into account via isospin-dependent slow rearrangement.[21] The nuclear density distribution is simulated by a step function distribution. There is no refraction for outgoing pions or protons, but the antinucleon is re-

fracted as it passes through the nucleus.

The successes of this approach are well documented.[19–22] It is perhaps the least model-dependent way in which to quantitatively determine what should happen in nuclear collisions under the assumption that the interaction proceeds as a series of incoherent hadron-hadron collisions. Of particular relevance to the $\bar{p}$-A energy deposition is ISABEL's ability to reproduce π-A scattering. The calculations reproduce the inelastic π scattering data and, most importantly, the "true" absorption data adequately for all observables considered here. Correlation measurements for π-A and presumably for $\bar{p}$-A require a more realistic description of the nuclear momentum distribution in terms of shell model wave functions.[23] Also, the lack of a realistic real optical potential for the pions introduces inaccuracies when comparison is made to exclusive final state measurements such as, again, correlations.

Another question concerns the nucleon mean free path (mfp) in nuclei. We have calculated 800 MeV proton $+^{40}$Ca inclusive proton spectra with ISABEL and found good agreement with the data of Ref. 24. This has been verified by more extensive calculations.[25] It must be noted that there is some controversy over "measured" versus calculated mfp's for nucleons in nuclei.[26,27] The INC mfp's range between 3 to 5 fm, depending on energy, while some "measurements" appear to give 5 to 7 fm. However, the interpretation of the data and the extraction of a mfp is not straightforward.[27] For the purposes at hand, we feel that the ability of ISABEL to reproduce pion-nucleus, nucleon-nucleus, and nucleus-nucleus inclusive proton spectra makes the extension to $\bar{p}$-A interactions valid. The physics, after all, is the same once the annihilation-produced pions scatter and create energetic nucleons and pions.

V. MODIFICATION OF ISABEL FOR $\bar{p}$-A INTERACTIONS

For antinucleons of kinetic energy $T_{\bar{N}}$ (GeV), the following parametrizations were employed:

$$\sigma_T^{\bar{N}N}(\text{mb}) = \exp[4.5485 \exp(-0.0601 \ln T_{\bar{N}})] , \quad (1)$$

$$\sigma_{\text{el}}^{\bar{N}N}(\text{mb}) = \exp[4.6052 - 1.0365 \exp(0.380 \ln T_{\bar{N}})] , \quad (2)$$

$$\sigma_{\text{cx}}^{\bar{p}p \to \bar{n}n}(\text{mb}) = 4.40/\sqrt{T_{\bar{N}}} , \quad (3)$$

$$\frac{d\sigma}{dt} = e^{bt} , \quad (4a)$$

$$b = 12.94 + 39.03 \exp(-2.075 P_{\text{lab}}) , \quad (4b)$$

where t is four momentum transfer $(\text{GeV}/c)^2$ and P_{lab} is the laboratory antiproton momentum in GeV/c. These parametrizations result from fits to data of Refs. 28 and 29 and appear as the solid lines in Figs. 1 and 2. They are valid for 100 MeV $< T_{\bar{p}} < 3$ GeV.

When an annihilation occurs, the characteristics are determined from the input at-rest multiplicity distribution of Ref. 30, distributed in charge according to the statistical phase space model of Orfanidis and Rittenberg,[11] and distributed uniformly in phase space, conserving E and p. The results reproduce the distribution[31] shown in Fig. 3. This model also yields a good description of the various annihilation branches (see Fig. 1 of Ref. 11). Use of the at-rest multiplicity and annihilation final state distributions limits the code to a range of $T_{\bar{p}} < 500$ MeV.

Because of the very strong attraction between $\bar{p}$'s and nuclei, care was taken to assure that the potential gradient at each refraction "shell" in the calculations was small. The far periphery of the nucleus was included by using 16 step regions and extending the last shell to 3.5 fm beyond the sharp cutoff radius of the nuclei considered. This latter fact is important for such a strongly absorbed projectile. The input characteristics were checked by calculating $\bar{p}p$ and $\bar{p}n$ reactions with the code.

VI. SOME CAUTIONS AND LIMITATIONS

No evaporation calculations were performed, so the proton spectra below $\simeq$40 MeV are not shown. Lack of nuclear refraction for pions and protons makes calculation of exclusive observables such as correlations unreliable, and thus they are not discussed in the present work.

It is interesting to note that the strong forward peaking of $d\sigma/dt$ results in most elastic and charge exchange $\bar{p}p, \bar{p}n$ events being Pauli blocked. The calculated $\bar{p}$ inelastic spectrum is then quite sensitive to the details of the nuclear Fermi distribution. The Fermi gas model is known to be inadequate in the nuclear surface,[32] so the inelastic $\bar{p}$-A scattering calculated via the INC using the Fermi gas model is unreliable. It is possible[23] to remedy this, and we are in fact pursuing this in conjunction with improvements that will allow us to also examine correlations.

It is important to realize that, in these calculations, a more realistic treatment of pion-nucleus op-

tical effects would only *increase* the energy deposition. The calculations should, if anything, underestimate the energy deposition.

VII. RESULTS

We have calculated 17 500 cascades for 175 MeV $\bar{p}+{}^{12}C$ and 19 000 for $\bar{p}+{}^{238}U$. These two target nuclei represent a compromise between cost and the desire to investigate the mass dependence of $\bar{p}$ annihilation on nuclei.

In examining the results, we concern ourselves with the following questions:

(a) Is there a large energy deposition $E_{\rm dep}$ a significant fraction of the time? Here

$$E_{\rm dep} \equiv m_p + m_{\bar{p}} + T_{\bar{p}} - \sum_{i=1}^{N} E_{\pi_i} , \tag{5}$$

where the sum includes all (N) pions that exit the nucleus. This definition has the advantage of being intuitively simple. It represents a lower limit when compared to alternate definitions which might, for example, subtract only the energies of "primordial" pions in Eq. (5).

(b) Do the antiprotons penetrate a significant distance into the nucleus before annihilating? This point is necessarily related to (a) and will be addressed in that context.

(c) What are the general observable characteristics of antiproton annihilations in nuclei?

(d) What are the characteristics of the high energy deposition events? Can they be easily distinguished from surface annihilations via an experimental trigger?

(e) The INC calculations are based on the assumption that nothing unusual is occurring. Can we, then, identify experimental quantities which are most likely to reflect the presence of degrees of freedom not included in the calculations?

Although we present our results from our particular perspective, we include as much information as space permits. Thus, investigators with other interest in $\bar{p}+A$ annihilations should find relevant results of the calculations in one of the sections below.

A. Energy deposition

In Figs. 4(a) and (b), we see the distribution of annihilation events versus $E_{\rm dep}$ for ^{12}C and ^{238}U, respectively. The error bars are statistical. To understand these results, recall that the pion can transfer energy to the nucleus in two ways:

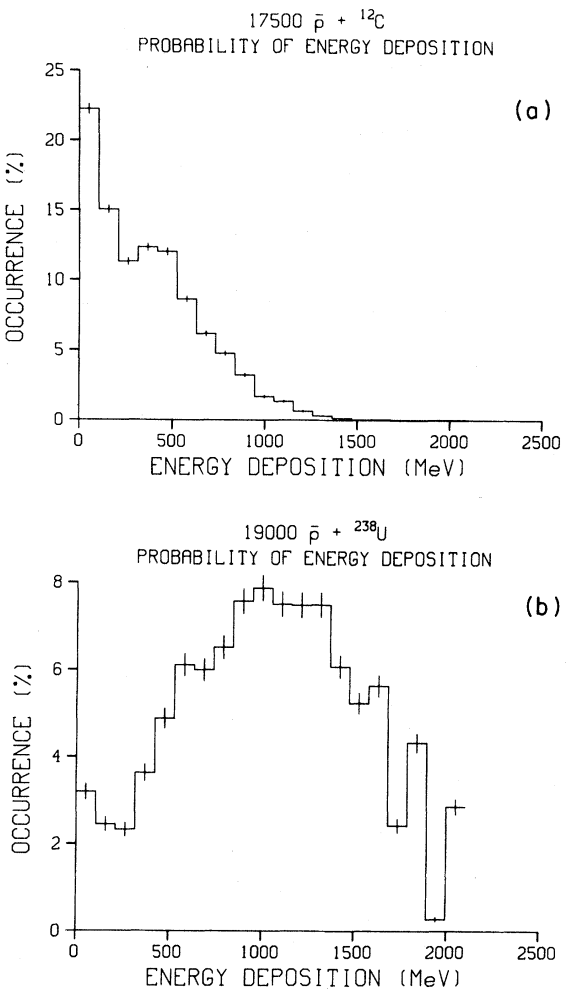

FIG. 4. (a) Probability of $\bar{p}$ annihilation in ^{12}C vs energy deposition ($E_{\rm dep}$) where $E_{\rm dep}$ is defined in Eq. (5). (b) The same quantity for ^{238}U. The bars represent the standard deviation of the distribution.

$$\pi + N \rightarrow \Delta , \qquad \Delta + N \rightarrow N + N + \pi ; \tag{6a}$$

$$\pi + N \rightarrow \Delta , \qquad \Delta + N \rightarrow N + N . \tag{6b}$$

In (6a), the Δ scatters about, distributing energy to the nucleons from which it recoils. In (6b), the π is "truly absorbed," i.e., the total energy of the pion ($m_\pi + T_\pi$) is given to two (or more) target nucleons. The latter process is quite efficient at depositing energy in the nucleus. The cross section for (6b) is, as noted earlier, significant and energy dependent.

Process (6b) is visible as a threshold effect in Figs. 4(a) and (b). The energy deposited by (6a) is rather smoothly distributed, while the absorption of one, two, three, . . . , pions is manifest as steps in E_{dep} on the order m_π. In Fig. 4(b), for example, we see a relatively large probability of all pions being absorbed ($2000 \leq E_{\text{dep}} \leq 2100$ MeV). The next lower interval (1900–2000) has few events because E_{dep} must drop by at least m_π (140 MeV) if one pion escapes. The increased probability for $1800 \leq E_{\text{dep}} \leq 1900$ reflects the "one escaped pion" events, and similar structure occurs when one pion is absorbed.

The peaks in E_{dep} at 400 MeV for ^{12}C and 1000 MeV for ^{238}U indicate that the average number of pions absorbed is 1 and 2, respectively. (Recall that for $\bar{N}N$ annihilations one gets on the average five pions, each with total energies of approximately 400 MeV.) The really striking result here is that for annihilations on ^{238}U, over 55% of the events result in $E_{\text{dep}} > 1$ GeV. For ^{12}C, 75% and for ^{238}U, 3% of the annihilations result in $E_{\text{dep}} > E_{\text{bind}}$ where $E_{\text{bind}} \sim 8A$ MeV.

Figure 5 shows E_{dep} versus the radius of annihilation. The bars indicate the standard deviation from the mean, not statistical errors. The crossed arrows indicate average values. As we expect, the large E_{dep} annihilations occur deeper within the nucleus.

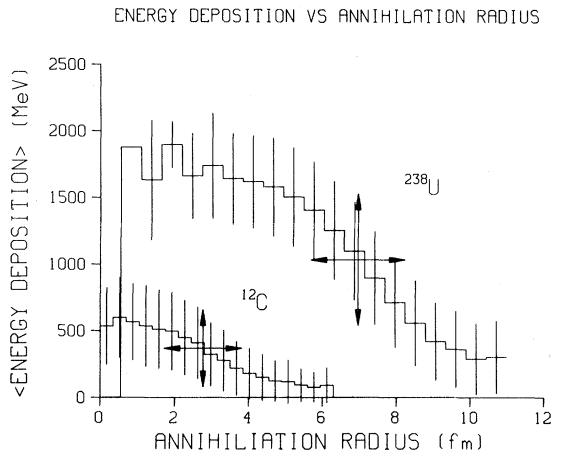

FIG. 5. Energy deposition [see Eq. (5)] from $\bar{p}$ annihilation in ^{12}C and ^{238}U vs the radius at which the annihilation occurs. The bars represent the width of the distribution of events. The crossed arrows indicate average values. The average annihilation radii are approximately equal to the nuclear sharp cutoff radii ($1.128\,A^{1/3}$), within 0.2 fm.

B. Penetrability

The annihilation probability versus annihilation radius is given in Figs. 6(a) and (b). The solid curves are calculations for a real $\bar{p}+A$ attractive potential of $V_R = 250$ MeV, while the dashed curves represent $V_R = 0$. The effect of the potential is to move the average annihilation radius farther into the nucleus, approximately 0.5 fm in each case. For both ^{12}C and ^{238}U, about 40% of the annihilations occur inside of the nuclear half-density radius. An appreciable fraction annihilate even further inside, although effectively no annihilations occur at the center (only 3% in ^{12}C and 0.01% in ^{238}U annihilate inside 1 fm). Penetration into regions of max-

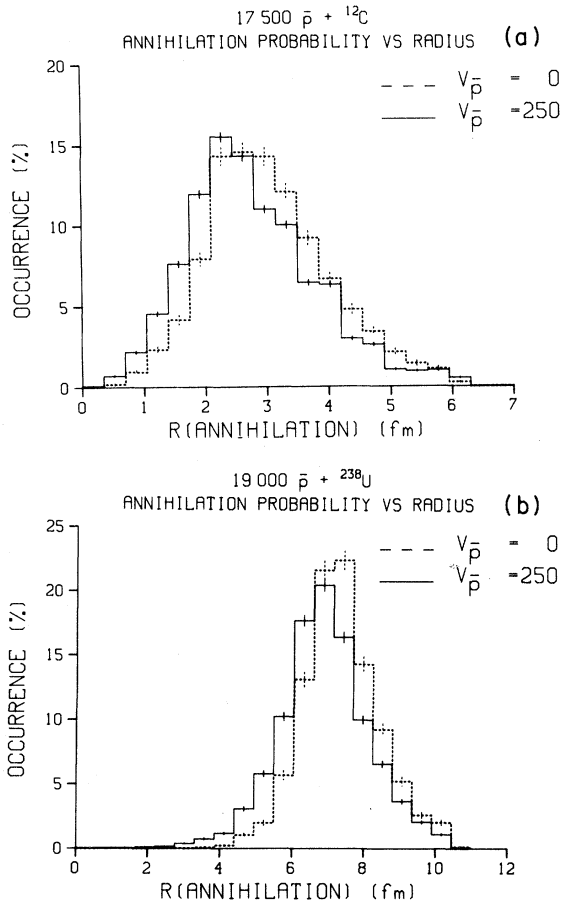

FIG. 6. (a) The probability of $\bar{p}$ annihilation in ^{12}C vs the radius of annihilation. The solid curve results from calculations with $V_R = 250$ MeV, the dashed curves with $V_R = 0$. (b) The same for ^{238}U. The bars are statistical errors. Note that $\simeq$50% of the annihilations occur within the sharp cutoff radii (7.0 fm for ^{238}U and 2.6 fm for ^{12}C). The effect of the potential in increasing the $\bar{p}$ penetrability is quite apparent.

imum density is important, however, in that interesting things are predicted to happen[2] when high energy densities occur in nuclear matter.

C. General characteristics

In this section we present pion and proton angular, energy, and multiplicity distributions for impact parameter averaged annihilations. Total reaction cross sections are also presented. All angles and energies are in the laboratory frame.

In Table I, the total reaction cross sections are presented. The reaction cross sections (σ_R) are given for $V_R=0$ and 250 MeV. The σ_R are, as expected, larger for the more attractive potential and increase as $A^{2/3}$, as should be the case for strongly absorbed projectiles.

Table II gives average multiplicities ($\langle n \rangle$) for pions, protons, and neutrons for $\bar{p}p$ at rest, $\bar{p}+{}^{12}$C, $\bar{p}+{}^{238}$U at 175 MeV, and $\bar{n}$-A (light nuclei) at 750 MeV. Note that, on the average, one pion is totally absorbed by ^{12}C and two pions by ^{238}U. The $\bar{n}$-A data are at a higher energy where inelastic π production is possible; thus the $\langle n_{\pi^+} \rangle$ is slightly larger than for $\bar{p}p$ at rest. The $\bar{n}$-A $\langle n_p \rangle$ is almost twice that for $\bar{p}+{}^{12}$C primarily due to the fact that our calculations do not include (slow) evaporation. If one examines the data of Ref. 13 and excludes protons below $\simeq$40 MeV, then $\langle n_p \rangle \simeq 1$.

In Figs. 7(a) and (b), the energy integrated angular distributions for π^+ and π^- are presented. The isotropic nature of the scattering, particularly for ^{238}U, underscores the uniqueness of the low-energy $\bar{p}+A$ interaction. Unlike high-energy A-A collisions, there is no projectile fragmentation to carry off momentum and energy. The decrease in $d\sigma/d\Omega$ at small angles is due to the attenuation of most forward going pions by the bulk of the nucleus. In Figs. 8(a) and (b) the proton and neutron distributions are shown. The pion, and particularly the nucleon angular distributions, indicate that ^{238}U thermalizes the deposited energy better than ^{12}C.

The angle integrated energy spectra are shown in Figs. 9(a) and (b) for π^+ and π^- and in Figs. 10(a) and (b) for protons and neutrons. The pion distributions have two components, a broad bump centered at about 300 MeV and a sharp peak at $\simeq$100 MeV. The lowest energy pions are essentially total-

TABLE I. Total reaction cross sections (σ_R) for $E_{\bar{p}}=175$ MeV. V_R is the strength of the (attractive) real optical potential whose shape follows the matter distribution.

	$\bar{p}+{}^{12}$C	$\bar{p}+{}^{238}$U
σ_R ($V_R=250$ MeV)	535 mb	2705 mb
σ_R ($V_R=0$)	420 mb	2290 mb

TABLE II. Average multiplicities from $\bar{p}$-p and $\bar{p}$-A annihilations. Columns two and three are the results of present calculations with $E_p=175$ MeV and $V_R=250$ MeV.

	$\bar{p}p$ at rest (Ref. 29)	$\bar{p}+{}^{12}$C	$\bar{p}+{}^{238}$U	$\bar{n}$-A 1.4 GeV/c (Ref. 13)
$\langle n_{\pi^\pm,0} \rangle$	5.0	4.1	2.9	
$\langle n_{\pi^+} \rangle$	1.5	1.1	0.7	1.59±0.06
$\langle n_{\pi^-} \rangle$	1.5	1.4	1.1	1.23±0.04
$\langle n_{\pi^0} \rangle$	2.0	1.6	1.1	
$\langle n_p \rangle$		1.0	2.9	2.12±0.09
$\langle n_n \rangle$		1.1	5.7	

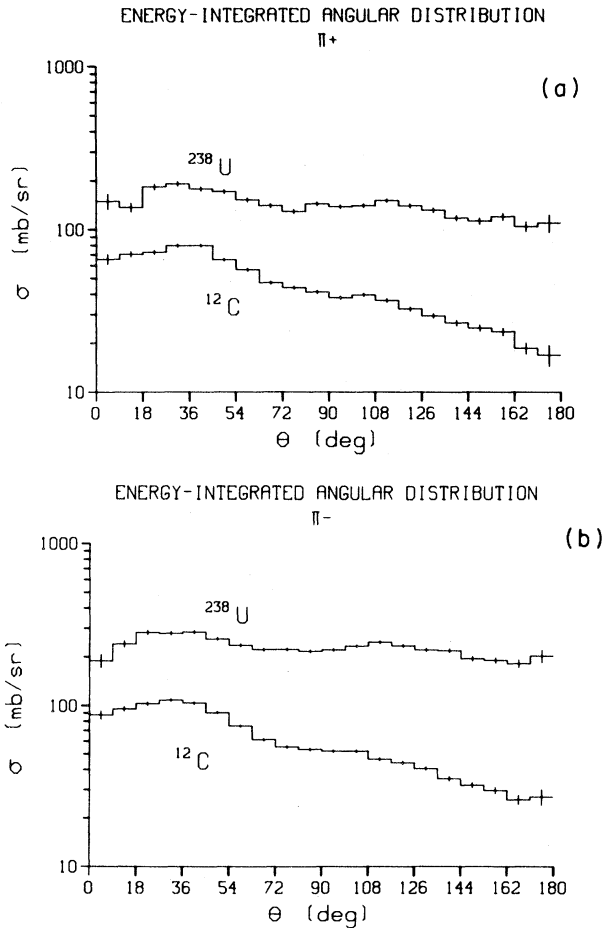

FIG. 7. (a) The energy integrated angular distributions for π^+ (vs laboratory angle) which result from $\bar{p}+{}^{12}$C, ^{238}U annihilations. (b) The same for π^-.

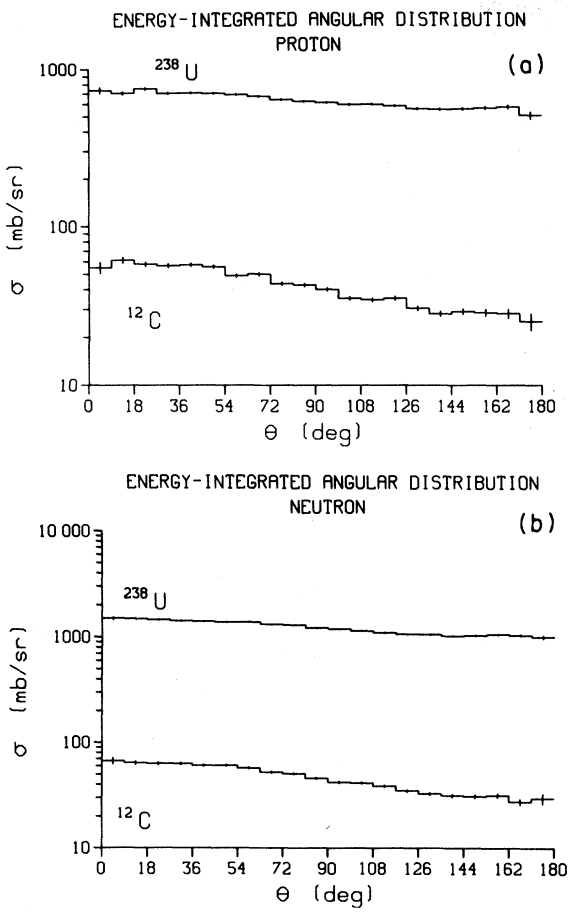

FIG. 8. (a) The energy integrated angular distributions for protons (vs laboratory angle) which result from $\bar{p}+{}^{12}C$, ${}^{238}U$ annihilations. (b) The same for neutrons.

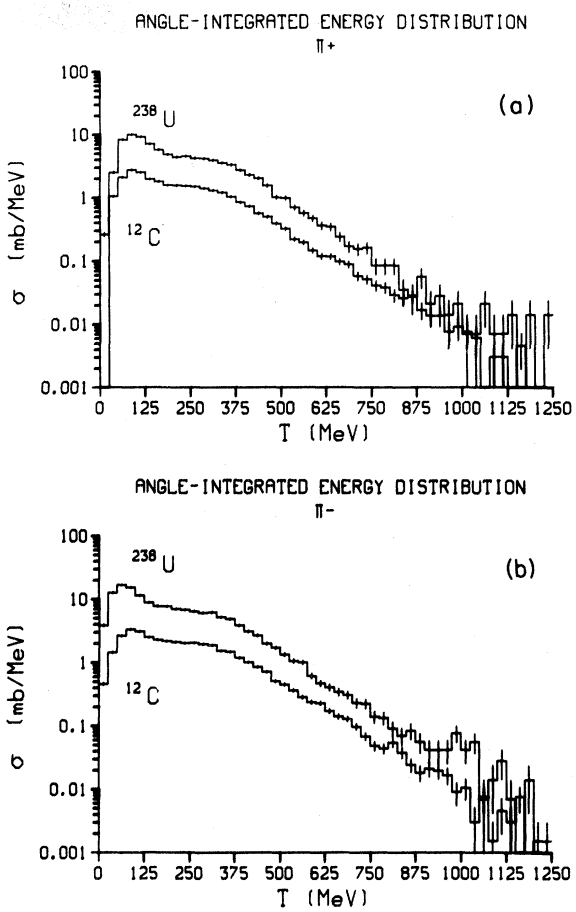

FIG. 9. (a) The angle integrated energy distributions for π^+ (vs laboratory kinetic energy) emitted in $\bar{p}+{}^{12}C$, ${}^{238}U$ annihilations. (b) The same for π^-. Note the "double bump" structure (see text) and the Coulomb effects at low T.

ly absorbed. Later, when we look at the pion energy spectra as a function of annihilation radius, it will become apparent that the two peaks correspond to primordial (i.e., relatively unaffected by nuclear scattering) and "secondary" pions.

The proton and neutron energy spectra [Figs. 10(a) and (b)] are relatively featureless. The slopes can be associated with a "temperature," or slope parameter, T_0:

$$d\sigma/dE \propto \exp(-T/T_0)\,. \tag{7}$$

For ${}^{238}U$ we find T_0 (proton)$=75$ MeV, while T_0 (neutron)$=68$ MeV. The corresponding values for ${}^{12}C$ are T_0 (proton)$=82$ MeV and T_0 (neutron)$=82$ MeV. Without ascribing too much significance to such a simple parametrization, we may compare these to inclusive proton spectra slope parameters obtained from nucleus-nucleus collisions.[1] We find that $T_0 \simeq 80$ MeV is observed in inclusive proton spectra from nucleus-nucleus collisions of approximately 1 GeV/nucleon laboratory energy.

Figures 11 and 12 show the doubly differential cross sections for π^+ and protons. The π^- and neutron spectra (not shown) are quite similar to π^+ and protons (respectively). Again the isotropy stands out. The pion spectra reveal an excess of higher energy pions at forward angles. The source of the ejectiles is more apparent in a rapidity plot, so the π^+ data are presented as a function of rapidity and perpendicular momentum in Fig. 13.

The proton and neutron rapidity plots (not shown) are quite featureless, showing only the isotropy apparent in Fig. 12. The pion rapidity plots are more interesting. We see that a large component of the pion spectrum emanates from the target ($Y=0$). There is, however, a component which has $Y \simeq -0.4$ from ${}^{12}C$ and $Y \simeq -0.6$ from ${}^{238}U$. These correspond to "backsplash" pions, or those

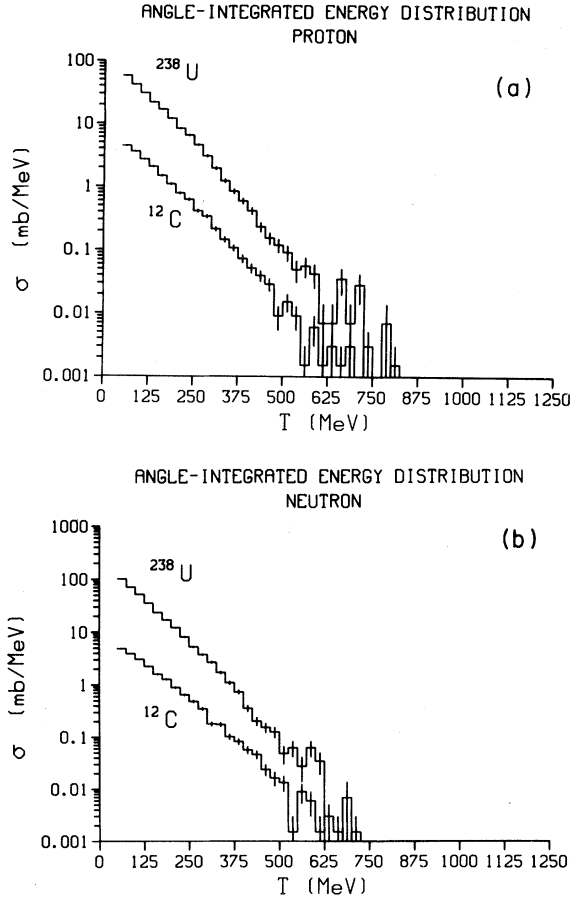

FIG. 10. (a) The angle integrated energy distributions for protons (vs laboratory kinetic energy) emitted in $\bar{p}+^{12}C$, ^{238}U annihilations. (b) The same for neutrons.

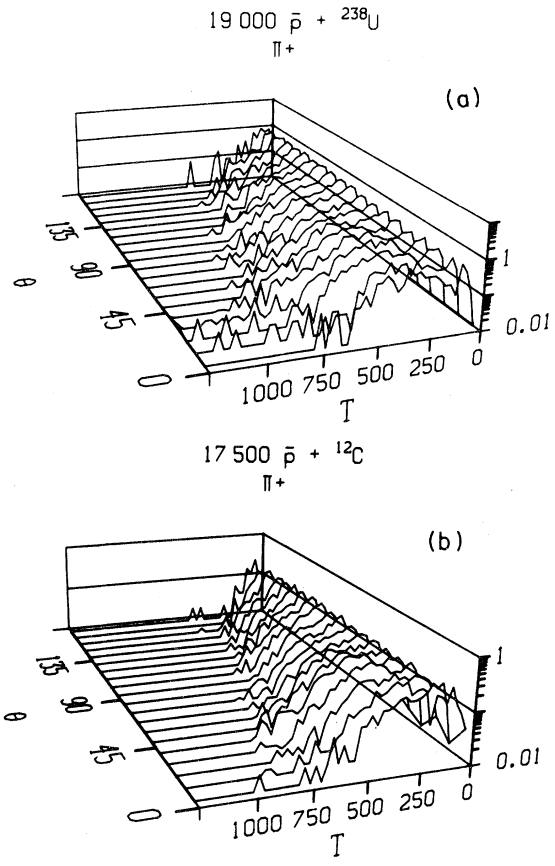

FIG. 11. (a) Doubly differential cross sections

$$\frac{d^2\sigma}{d\Omega\, dT_\pi}(\text{mb/MeV sr})$$

for π^+, resulting from $\bar{p}+^{238}U$ and (b) $\bar{p}+^{12}C$ annihilations.

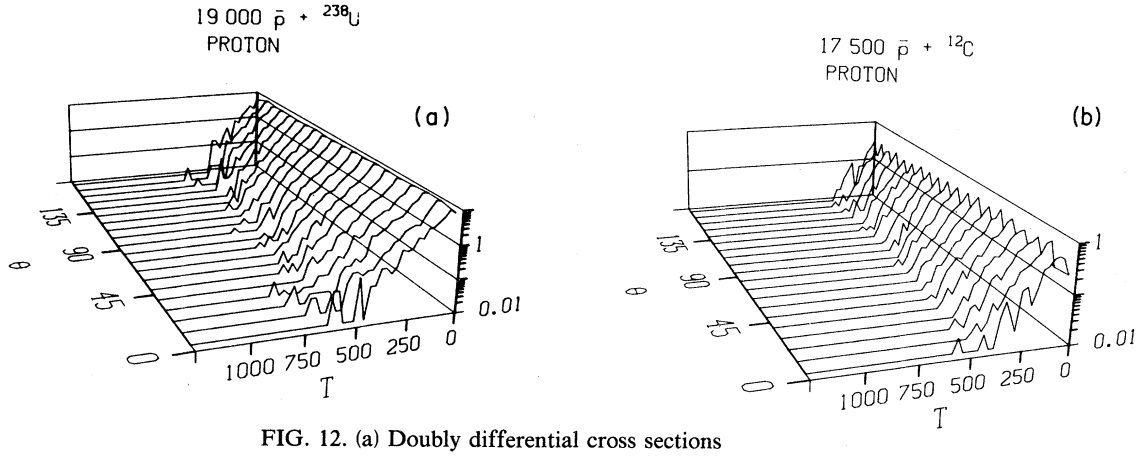

FIG. 12. (a) Doubly differential cross sections

$$\frac{d^2\sigma}{d\Omega\, dT_p}(\text{mb/MeV sr})$$

for protons resulting from $\bar{p}+^{238}U$ and (b) $\bar{p}+^{12}C$ annihilations.

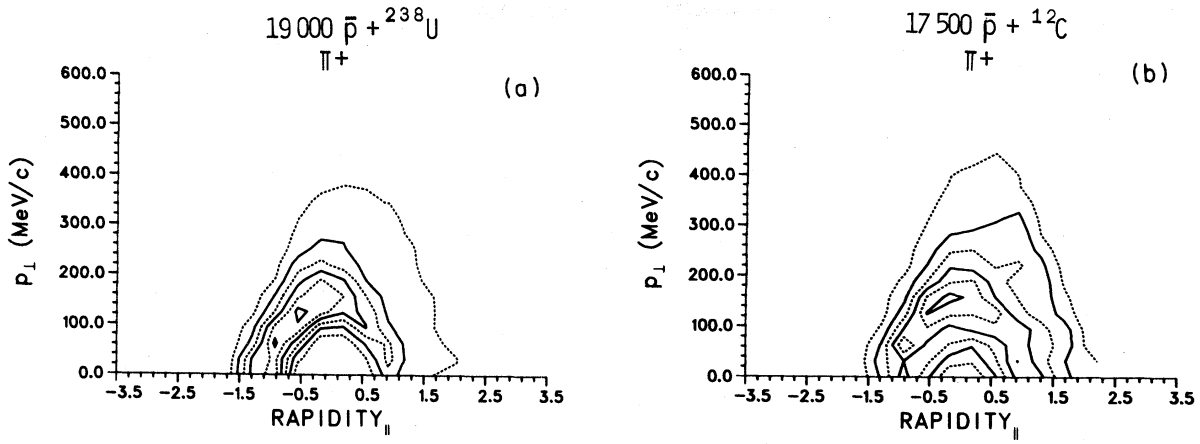

FIG. 13. (a) Longitudinal rapidity (Y) vs transverse momentum for π^+ emitted in $\bar{p}+^{238}$U and (b) $\bar{p}+^{12}$C annihilations. Note the backsplash pion peak at $Y\simeq -0.6$ and $P_\perp \simeq 100$ MeV/c. The solid contour intervals are 0.2 b/GeV^2 for ^{12}C and 0.9 b/GeV^2 for ^{238}U.

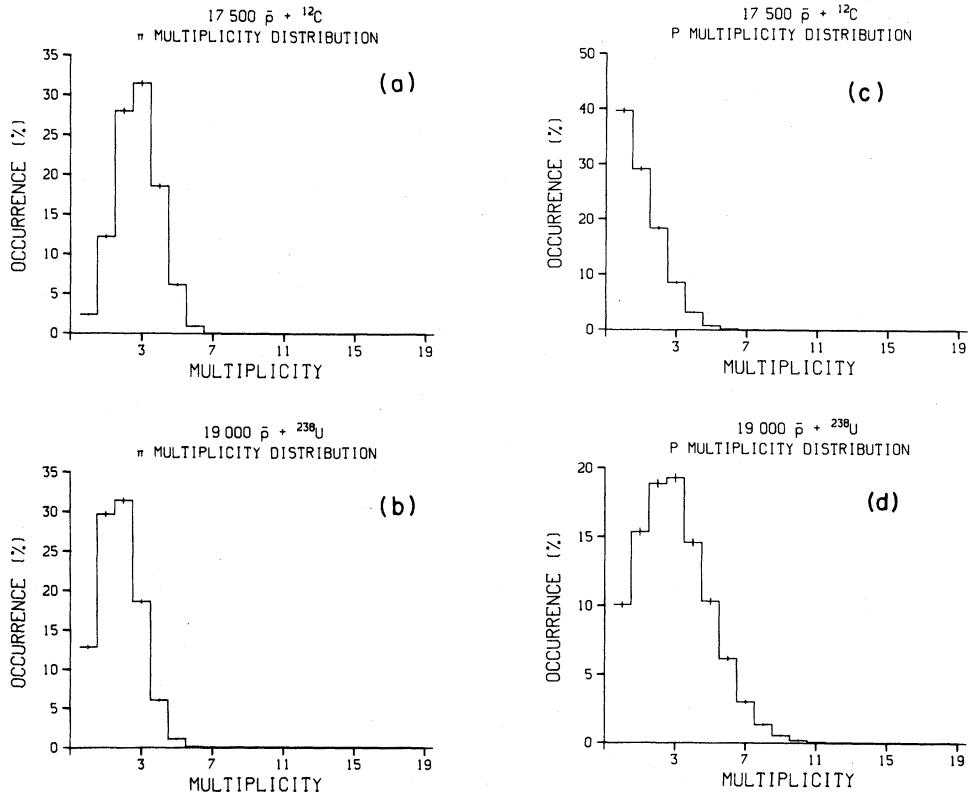

FIG. 14. (a) The resultant charged pion multiplicity distributions for $\bar{p}+^{12}$C annihilations and (b) for $\bar{p}+^{238}$U annihilations. (c) The resultant proton multiplicity distributions for $\bar{p}+^{12}$C and (d) $p+^{238}$U annihilations. The error bars are statistical.

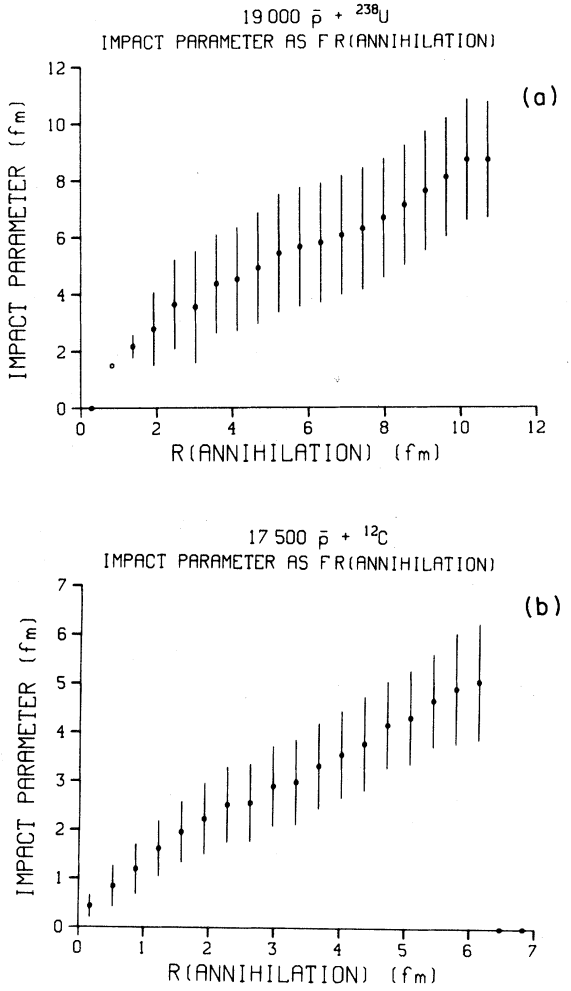

FIG. 15. (a) The impact parameter vs radius of annihilation for $\bar{p}+{}^{12}C$ and (b) $\bar{p}+{}^{238}U$ annihilations. The bars indicate the width of the distribution of events.

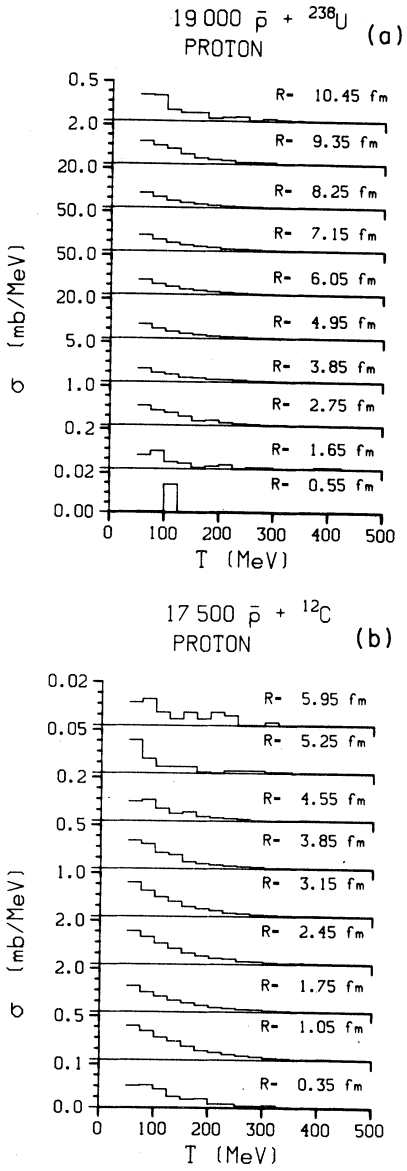

FIG. 16. (a) The angle-integrated energy distribution binned according to radius of annihilation for protons resulting from $\bar{p}+{}^{238}U$ and (b) $\bar{p}+{}^{12}C$ annihilations.

which move backward with little attenuation after the annihilation. The π^- rapidity plots (not shown) are similar to the π^+. These rapidity distributions are quite different from heavy ion collisions, for which are generally seen protons, neutrons, and pions associated with fragments having projectile, target, and (sometimes) center-of-mass rapidities. The lack of fragmentation in $\bar{p}$-A annihilations is quite apparent here.

In Fig. 14, we see the multiplicity distributions for charged pions [14(a) and (b)] and protons [14(c) and (d)]. Comparison with the free $\bar{p}p$ pion multiplicity distribution (inset Fig. 3) reveals the degree of pion attenuation for ^{12}C and ^{238}U. The proton multiplicity for ^{238}U can be quite large. As we shall see, large $\langle n_p \rangle$ is correlated with a large energy deposition.

Finally, in Figs. 15(a) and (b), the relationship between impact parameter (b) and annihilation radius is displayed. The strong attraction makes R_{ann} a more useful variable than b. This is reflected in the fact that a given R_{ann} can originate from a broad range of impact parameters.

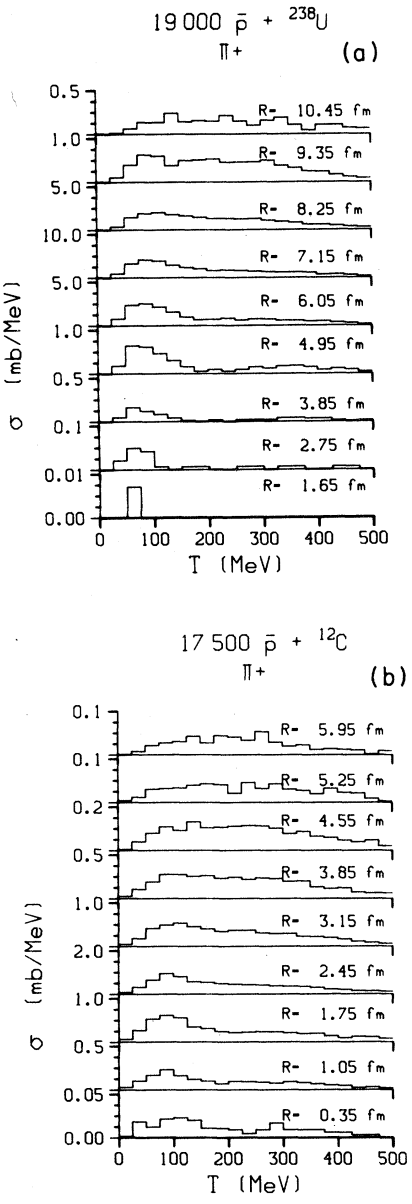

FIG. 17. (a) The angle-integrated energy distributions binned according to radius of annihilation for π^+ resulting from $\bar{p}+^{238}U$ and (b) $\bar{p}+^{12}C$ annihilations. Note the distinct appearance of two components in the spectra (see text).

D. Character of large E_{dep} annihilations

Assuming that nothing unusual is occurring, the method for energy deposition is pion scattering and absorption. The large E_{dep} annihilations will perforce happen deeper within the nucleus. In Figs. 16 and 17, we see the proton and π^+ angle integrated energy spectra for various radii of annihilation. The proton spectra are not particularly interesting, but the pion spectra reveal some structure. This "double bump" shape is also visible in Fig. 9. A broad distribution centered at approximately 200 MeV corresponds to primordial pions, mostly from peripheral annihilations. A lower energy peak arises as annihilations occur deeper within the nucleus. These "thermalized" pions seem to result from small R_{ann}, large E_{dep} annihilations. Thus examinations of those events with an excess of low energy pions should prove interesting.

Another large E_{dep} indicator is the pion and proton multiplicity. These can be seen in Fig. 18. There is, as one might expect, a particularly strong correlation between the number of protons ejected and the energy transferred to the nucleus. Similarly, there is an inverse correlation for the pions. Note that the bars in Fig. 18 indicate the standard deviation of events, not statistical errors.

Another possibility centers on the observation made earlier with reference to Fig. 13 concerning backsplash pions. The lack of such pions could indicate a relatively deep annihilation.

E. Deviations from INC behavior

It would be somewhat disappointing if the data agreed quite well with these calculations. One might hope that a significant number of annihilations would lead to new phenomena such as those envisioned by Rafelski,[33] where the annihilation fireball "melts" nearby nucleons to form a quark/gluon plasma. If such degrees of freedom are indeed open, how might these new channels be reflected in the observables discussed here?

Any answer depends, unfortunately, on the decay characteristics of the unknown "state." A rapid decay into pions would be difficult to distinguish, while decay into gamma rays would definitely upset the (assumed INC) energy balance. The most optimistic scenario would have the quark blob living for $>10^{-10}$ sec and being detected as a strange charge to mass ratio particle. In addition, the decay of a quark-gluon plasma into strange particles has been suggested.[33]

One might then look for a kaon yield over and above that expected simply from known $\bar{p}+p\rightarrow$ kaons and pions. We are in the process of calculating $\bar{p}+A\rightarrow$ kaon production for this purpose. Significant deviations from the INC predictions could

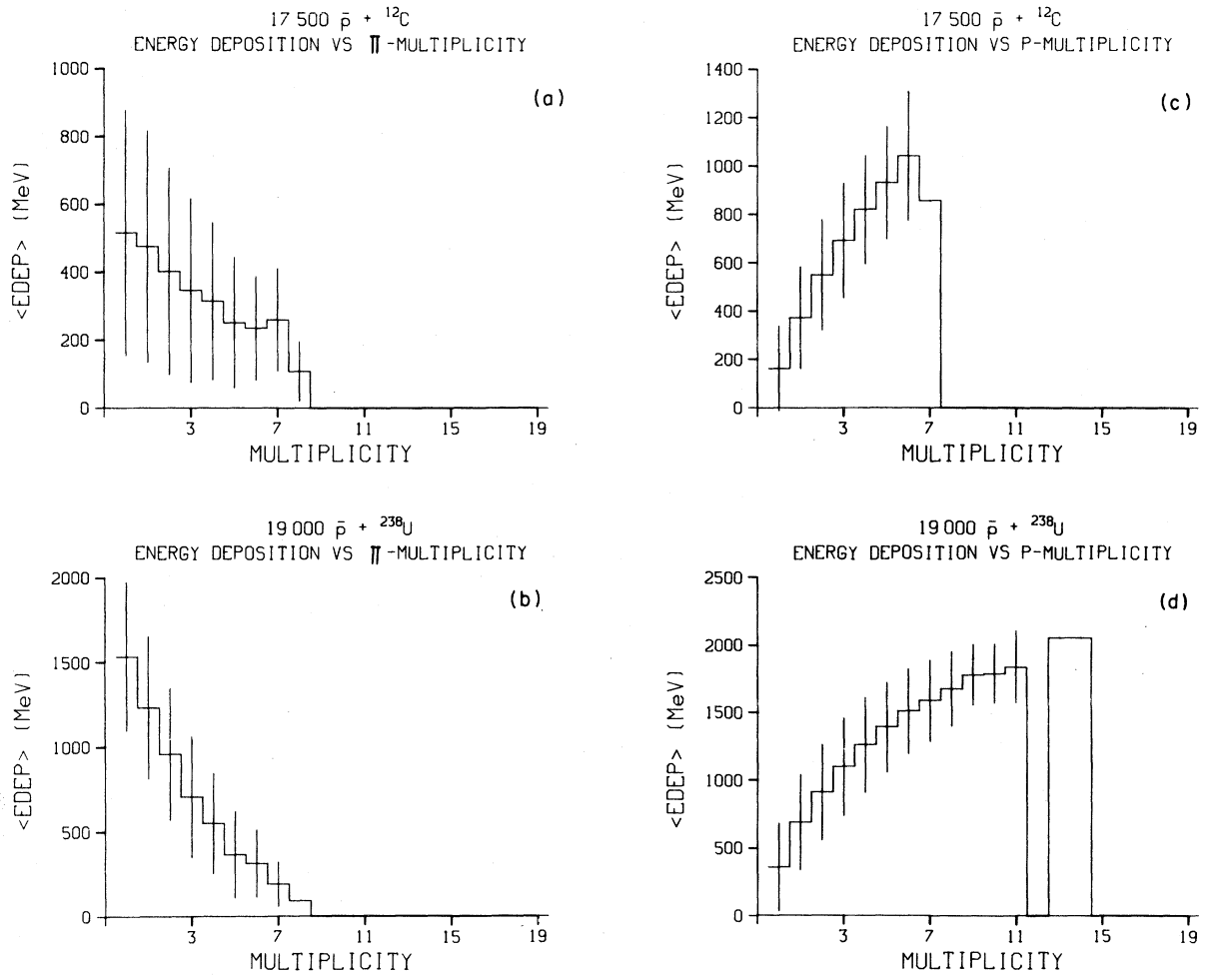

FIG. 18. Energy deposition (E_{dep}) as defined in Eq. (5) vs charged pion multiplicity for (a) $\bar{p}+^{12}C$ and (b) $\bar{p}+^{238}U$ annihilations. (c) E_{dep} vs proton multiplicity for $\bar{p}+^{12}C$ and (d) $\bar{p}+^{238}U$ annihilations.

indicate the presence of other degrees of freedom. For example the slope parameters extracted from Fig. 10 might be different. The isotropy might be upset if jetlike behavior occurred. Broad range proton and pion inclusive data are necessary for such comparisons. The shape of multiplicity distributions might also be affected.

Production of fragments in $\bar{p}$-A annihilation cannot be calculated in the present approach. However, thought must be given to examination of fragments, perhaps using the techniques of Ref. 4.

VIII. CONCLUSIONS

We have performed realistic calculations of $\bar{p}$-A interactions at low energies within the intranuclear cascade model. The results indicate that a large amount of energy can be transferred to the nucleus in a unique way. The characteristics of the annihilations of $\bar{p}$'s within nuclei are quite unlike anything seen in conventional hadron-nucleus and nucleus-nucleus collisions. These calculations should provide important background for comparison with data from upcoming LEAR experiments as well as lending insight into the nature of this fascinating area of nuclear physics.

ACKNOWLEDGMENTS

We are grateful to K. Hirons, M. Schirru, and the rest of the Los Alamos Central Computing Facility consulting staff for their patient assistance. This work was supported in part by the U. S. Department of Energy.

*Permanent address: Soreq Nuclear Research Center, Yavne 70600, Israel.

[1]Proceedings of Fifth High Energy Heavy Ion Study, Lawrence Berkeley Laboratory Report LBL-12652, 1981.

[2]Proceedings of First Workshop on Ultrarelativistic Nuclear Collisions, Lawrence Berkeley Laboratory Report LBL-8957, 1979.

[3]H. Stocker *et al.*, Phys. Rev. Lett. 47, 1807 (1981).

[4]R. W. Minich *et al.* (unpublished); J. E. Finn *et al.* (unpublished).

[5]J. Rafelski, Phys. Lett. 91B, 281 (1980); J. Rafelski, H.-Th. Elze, and R. Hagedorn, Proceedings of the Fifth European Symposium on $\bar{N}$-N Interactions, Bressanone, 1980.

[6]R. M. DeVries and N. J. DiGiacomo, Proceedings of the Workshop on Nuclear and Particle Physics at Energies up to 31 GeV: New and Future Aspects, Los Alamos Scientific Laboratory Report LA-8775-C, 1981, p. 541.

[7]See CERN Gray book: Experiments at CERN, 1982, CERN, Geneva, 1982 (unpublished).

[8]N. J. DiGiacomo, J. Phys. G 7, L169 (1981); N. J. DiGiacomo and R. M. DeVries, Proceedings of the Workshop on Nuclear and Particle Physics at Energies up to 31 GeV: New and Future Aspects, Los Alamos Scientific Laboratory Report LA-8775-C, 1981, p. 547.

[9]A. I. Yavin (unpublished).

[10]M. Deutschmann *et al.*, Nucl. Phys. B103, 198 (1976).

[11]S. J. Orfanidis and V. Rittenberg, Nucl. Phys. B59, 570 (1973); A. M. Cooper *et al.*, *International Symposium on $\bar{N}N$ Interactions, Proceedings of the Stockholm Symposium, 1976* (Pergamon, New York, 1977).

[12]A. K. Ekspong *et al.*, Nucl. Phys. 22, 353 (1961).

[13]H.-J. Besch *et al.*, Z. Phys. A 292, 197 (1979).

[14]L. Agnew *et al.*, Phys. Rev. 118, 1371 (1960).

[15]P. D. Barnes *et al.*, Phys. Rev. Lett. 29, 1132 (1972); P. Roberson *et al.*, Phys. Rev. C 16, 1945 (1977); H. Poth *et al.*, Nucl. Phys. A294, 435 (1978).

[16]H. Aihara *et al.*, Nucl. Phys. A360, 27 (1981).

[17]W. W. Buck, C. B. Dover, and J. M. Richard, Ann. Phys. (N.Y.) 121, 47 (1979); C. B. Dover and J. M. Richard, *ibid.* 121, 70 (1979).

[18]E. Auerbach, C. B. Dover, and S. H. Kahana, Phys. Rev. Lett. 46, 702 (1980).

[19]K. Chen, G. Friedlander, G. D. Harp, and J. M. Miller, Phys. Rev. C 4, 2234 (1971); G. D. Harp *et al.*, *ibid* 8, 581 (1973).

[20]Y. Yariv and Z. Fraenkel, Phys. Rev. C 20, 2227 (1979).

[21]Y. Yariv and Z. Fraenkel, Phys. Rev. C 24, 488 (1981).

[22]J. Ginocchio, Phys. Rev. C 17, 195 (1978).

[23]Z. Fraenkel, E. Piasetzky, and G. Kalbermann, Phys. Rev. C (to be published).

[24]J. McGill, thesis, Los Alamos Scientific Laboratory Report LA 8937-7, 1981.

[25]Z. Fraenkel, private communication.

[26]J. P. Schiffer, Comm. Nucl. Part. Phys. 10, 243 (1981).

[27]R. M. DeVries and N. J. DiGiacomo, J. Phys. G 7, L51 (1981).

[28]CERN-HERA Report 79-03, 1979.

[29]Lawrence Berkeley Laboratory Report LBL-58, 1972.

[30]J. Roy *et al.*, *Proceedings of the Fourth International Symposium on $\bar{N}N$ Interactions, Syracuse, 1975,* edited by T. E. Kalogeropoulos and K. C. Wali (Syracuse University, Syracuse, 1975).

[31]G. Ghesquire *et al.*, see Ref. 30.

[32]G. Bertsch and O. Scholten, Phys. Rev. C 25, 804 (1982).

[33]J. Rafelski, University of Frankfurt Report UFTP-73/1982, 1982; J. Rafelski and B. Mueller, Phys. Rev. Lett. 48, 1066 (1982).